Soil Thermal Response to Temperature Cycles and End Boundary Conditions of Energy Piles

Mohammed Faizal

Research Fellow, Monash University, Department of Civil Engineering, 23 College Walk, Clayton, Vic. 3800, Australia. Telephone: +61399029988; Email: mohammed.faizal@monash.edu

Aria Moradshahi

PhD student, Monash University, Department of Civil Engineering, 23 College Walk, Clayton, Vic. 3800, Australia. Telephone: +61399058901; Email: aria.moradshahi@monash.edu

*** Abdelmalek Bouazza (Corresponding Author)**

Professor, Monash University, Department of Civil Engineering, 23 College Walk, Clayton, Vic. 3800, Australia. Telephone: +61399054956; Email: malek.bouazza@monash.edu

John S. McCartney

Professor and Department Chair, University of California San Diego, Department of Structural Engineering, 9500 Gilman Drive, La Jolla, CA 92093-0085, USA, Telephone: +18585349630; Email: mccartney@ucsd.edu

Abstract

This paper explores the influence of building cover and pile toe boundary conditions on ground temperature distributions surrounding energy piles. Experimental and numerical studies were conducted on two isolated cast-in-place energy piles installed in dense unsaturated sand, one exposed to the atmosphere at the ground surface (diameter = 0.6 m and length = 16.1 m) and the other installed under a six-story building (diameter = 0.6 m and length = 10 m). Investigations were conducted for monotonic heating and daily cyclic temperature changes of the piles ranging between 10°C and 35°C. The changes in ground temperature reduced with increasing radial distance from the edge of both piles. Cyclic temperatures in both piles induced lower ground temperature changes and decreased the radial thermal influence zone compared to monotonic heating. However, the radial thermal zone in cyclic operating mode can be influenced by different ratios of heating to cooling times and hence should be selected carefully to avoid unexpected ground temperature changes. Atmospheric effects were observed up to a depth of 2 m for the energy pile exposed to the atmosphere. The insulation provided by the building footprint slightly reduced the impacts of ground-atmosphere interaction on the soil temperature distribution with depth near the surface compared to the energy pile exposed to the atmosphere. The ground temperature variations were dominant along the length of the heat exchanger loops for both piles. Still, they were negligible near the pile toe below the heat exchanger loops for both piles.

Keywords: *Energy piles; temperature cycles; ground temperatures; radial thermal influence zone; end boundary conditions.*

Introduction

Energy piles have been implemented successfully in many countries since their first use in the 1980s (Brandl 2006, De Moel et al. 2010). However, despite the significant advances made in the past decade in understanding their thermo-mechanical behaviour, critical knowledge gaps remain that need to be addressed. In particular, the influences of temperature cycles and boundary conditions at the head and toe of energy piles on the ground temperature responses deserve further study.

Energy piles typically undergo monotonic and cyclic temperature changes depending on the heating/cooling requirements of the building. Cyclic temperatures result from seasonal operations or daily intermittent operations of the ground source heat pump (GSHP) (Brandl 2006; Yi et al. 2008; Wood et al. 2010; Dai et al. 2015; Faizal et al. 2016; Murphy and McCartney 2015; McCartney and Murphy 2017; Faizal et al. 2018; Faizal et al. 2019a). Furthermore, the presence of a building footprint overlying the energy piles could act as a thermal insulator which will minimize the effects of atmospheric temperature variations on the ground temperature (Murphy et al. 2015). This, in turn, could affect the geothermal energy source or sink available to the energy piles (e.g., Ghasemi-Fare and Basu 2018). Although anticipated to be minor, ground temperature changes below the toe of energy piles without groundwater flow could also affect the temperature distribution within the surrounding soils (Singh et al. 2015). The end boundary conditions of the energy pile could lead to variable amounts of geothermal energy accessed per unit length of the energy pile, which may affect the building thermal design.

Field studies conducted on isolated energy piles without the presence of building cover (Li et al. 2006; Bourne-Webb et al. 2009; You et al. 2014; Singh et al. 2015; Yu et al. 2015; Faizal and Bouazza 2018; Guo et al. 2018) and installed under buildings (Murphy et al. 2015; Chen et al. 2017) have generally indicated that soil temperature changes are most substantial near the pile and tend to reduce with increasing radial distance from the pile when the pile is subjected to monotonic temperature variations. There are, however, minimal studies conducted on the radial soil temperature distribution due to daily cyclic temperature changes at a field scale. The few field studies on daily temperature cycles available in the literature were conducted on energy piles without the presence of a cover provided by a building (e.g., Faizal et al. 2016; Faizal and Bouazza 2018). The temperature cycles evaluated in these studies led to lower ground temperature changes compared to monotonic temperature operations of the GSHP. Consequently, temperature cycles can thermally affect lower volumes of soils and reduce the radial thermal influence zones compared to monotonic temperatures. This, in turn, could reduce the likelihood of thermal interactions with nearby energy piles with lower thermal impacts on the surrounding soil for long term operations.

Natural ground temperatures (without energy pile operation) are commonly affected by atmospheric temperature fluctuations down to given depths when the ground surface is exposed to the atmosphere (e.g., Brandl 2006; Guo et al. 2018; Jalaluddin et al. 2011; Singh et al. 2015). Preliminary 1g physical model studies conducted by Ghasemi-Fare and Basu (2018) indicate that the presence of surface thermal insulation causes a reduction in the effects of ambient temperature fluctuations on the ground temperature responses. Murphy et al. (2015) also observed that near-surface ground temperatures below a floor slab were less affected by ambient temperatures than the ground without surface cover outside a building footprint. Kaltreider et al. (2015) performed numerical simulations of a building with energy piles and found that energy pile operation led to an increase in the floor slab heat loss from the building during the heating season. These preliminary observations highlight the fact that the presence of the building cover will affect the ground temperature distribution during energy pile operations. Therefore, findings from studies conducted on energy piles without building cover may not be directly translated to actual design and installations of energy piles under buildings.

This paper uses experimental and numerical evaluations of the soil thermal response surrounding two field-scale energy piles to examine the effects of temperature cycles and boundary conditions at the head and toe of the energy piles. Specifically, this study assesses the influence of monotonic and daily cyclic temperature changes of the energy piles and the effects of the building cover and near pile toe boundary conditions on the radial and vertical soil temperature distribution. Experiments on two separate field-scale energy piles (one exposed to the ground surface without an applied head load and another under a 6-story residential building) and numerical simulations were conducted to achieve the aims of this paper.

Site Details and Experimental and Numerical Procedures

Site Details

The two energy piles evaluated in this study were bored and cast-in-place in a similar soil formation within a distance of 500 m of each other. The soil profile at the location of both energy piles consisted of dense to very dense sands, which are part of the Brighton Group of materials; the thermal and mechanical properties of these soils are, therefore, expected to be similar. The soil types at the two sites are summarized in Tables 1 and 2 and are documented extensively in Barry-Macaulay et al. (2013), Singh et al. (2015), Wang et al. (2015), and Faizal et al. (2018; 2019a, b). There was no groundwater encountered within the depth of the piles at the two sites.

A schematic diagram of the energy piles, including the locations of the sensors, is shown in Figure 1. The full details of the instrumentation and installation procedures for both piles are documented in Wang et al. (2015), Singh et al. (2015), Yu et al. (2015), Wang (2017) and Faizal et al. (2018; 2019a, b). The piles were not precisely similar (e.g. same dimensions, same number of heat exchanger loops and the same locations of sensors in the piles and the surrounding soil) as they were installed for different purposes and at different times.

The unrestrained energy pile, installed in December 2010, was used to study the changes in shaft capacity by partially translating the upper 10 m section after thermal loading using two Osterberg Cell (O-Cell) load testing systems at depths of approximately 10 m and 14 m (Wang et al. 2015; Wang 2017). The building under which the restrained energy pile was installed was completed in December 2015. The restrained energy pile is from a pair of two energy piles spaced at a center-to-center distance of 3.5 m and was the only thermally active pile evaluated for the purpose of this paper. Although the diameters of the restrained and unrestrained energy piles were the same (0.6 m), they both had different lengths. The unrestrained energy pile was 16.1 m long, whereas the restrained energy pile was 10 m long. The head of the unrestrained energy pile was level with the ground surface and was exposed to the atmosphere, while the head of the restrained energy pile was integrated into the building slab.

High-density polyethylene (HDPE) pipes with outer and inner diameters of 25 mm and 20 mm, respectively, were used to form U-loop heat exchangers that were attached to the vertical reinforcement bars in the reinforcement cages of the energy piles. The HDPE pipes and sensors were installed in the reinforcement cages before lowering the cages in the drilled holes. Concrete was poured slowly using tremies to avoid possible damage to the sensors. There were three evenly distributed U-loops installed up to a depth of 14.2 m in the unrestrained energy pile (Figure 2a). In contrast, the restrained energy pile had four evenly distributed U-loops installed to the full depth of the energy pile (Figure 3a). The spacing between the pipe loops in the unrestrained and restrained energy piles was approximately 175 mm and 200 mm, respectively. Since the HDPE pipes were attached to the vertical reinforcement bars in the pile cage, the spacings between the loops remained constant along the pile length.

The concrete mixes and the compressive strengths of the concrete in the two energy piles were similar. The concrete mix of the unrestrained energy pile consisted of 7 mm aggregates, cement, and fly ash with a water to cement ratio of 0.45. The average compressive strengths of unreinforced concrete samples were 40.9 and 65.6 MPa after 35 and 210 days, respectively. The concrete used in the restrained energy pile consisted of 7 mm aggregated cement, slag, and fly ash with a water to cement ratio of 0.42. The compressive strengths of unreinforced concrete samples were 40 and 62 MPa after 7 and 33 days of installation, respectively.

For each of the energy piles, the surrounding soil temperatures were monitored in boreholes located at two radial distances, *R*, from the edge of the energy piles (Figure 1). In the case of the unrestrained pile, the boreholes (16 m long) were at R = 0.5 m and R = 2 m; type K thermocouples were used to monitor the changes in temperature. For the restrained pile, up to a depth of 12 m, the boreholes were at R = 0.63 m and R = 1.95 m, respectively; the temperature was monitored using type T thermocouples. The inlet/outlet fluid temperatures of the unrestrained energy pile were recorded at the pile head. In contrast, the restrained energy pile fluid temperatures were recorded at the inlet/exit of the plumbing manifold located approximately at 15 m in a plant room where the heating/cooling equipment was stored. The fluid flow rates were recorded using TM series digital flowmeters installed at the exit of the heating/cooling units. The pile temperatures were monitored using vibrating wire strain gauges (VWSGs) (Geokon, NH, USA) installed at different depths, as shown in Figure 1. The VWSGs were capable of measuring both temperatures and strains. The atmospheric air temperatures were extracted from the online data bank of the nearest weather station located approximately 13 km from the experimental sites for the duration of all the experiments.

Experiments

The two energy piles were subjected separately to monotonic heating and daily cyclic temperatures. The effects of cyclic temperature changes were examined by cooling the energy piles for 16 hours followed by 8 hours of heating daily, simulating forced ground thermal recharging of a solar hybrid GSHP system for a scheduled intermittent mode of operation.

The monotonic heating experiments were conducted using a GeoCube thermal response test (TRT) unit. The cyclic temperature experiments of the unrestrained energy pile were conducted using two pieces of equipment; a United Refrigeration chiller for cooling for 16 hours followed by heating for 8 hours using a GeoCube TRT unit. Water was used as the heat transfer fluid in these experiments. The cyclic temperature experiment of the restrained energy pile was conducted using a commercial 2-5 kW Envision geothermal/water source heat pump by switching between cooling and heating modes. In this experiment, the heat transfer fluid was a mixture of a Fernox Alphi-11 antifreeze protector added at approximately 25% of the total volume of water in the system to avoid any possible freezing during the cooling cycle. The four experiments, summarized in Table 3, were conducted for a different number of days; only 16 days of data are presented in this study for the sake of comparison and clarity. Some of the field data used to validate the numerical models and to meet the objectives of this study were available from previous studies performed on the two energy piles (Singh et al. 2015; Yu et al. 2015; Wang et al. 2015; Faizal et al. 2018; Faizal and Bouazza 2018; Faizal et al. 2019a; 2019b).

The temperatures of the fluids entering the energy piles and daily atmospheric temperatures are shown in Figure 4. Due to the high inlet fluid temperatures, the fluid flow to the inlet of the unrestrained energy pile was stopped multiple times at the beginning of each cycle to control water temperatures in the tanks of the heating/cooling units before re-establishing flow (Figure 4a). This is because the water temperatures from each cycle affected the next cycle throughout the experiments when switching between cooling and heating cycles.

There were some performance issues of the heat pump at the start of the cyclic temperature experiments for the restrained energy pile; this led to a cooling time of 26 hours in the first cooling cycle, while the other cooling cycles were 16 hours, followed by 8 hours of heating (Figure 4b).

The inlet fluid temperatures during monotonic heating reached up to 45 and 48°C for the unrestrained (Figure 4a) and restrained energy piles (Figure 4b), respectively, while the atmospheric temperatures ranged from 15 – 25°C (Figure 4c) and 12 – 26°C (Figure 4d), respectively. The inlet fluid temperatures for cyclic experiments ranged from 8 – 30°C for the restrained energy pile. For cyclic experiments of the unrestrained energy pile, the inlet fluid temperatures ranged from 7 – 16°C during cooling and 30 – 55°C during heating. As a result of using different equipment when testing the two energy piles, the ranges of inlet fluid temperatures between the two energy piles were different, particularly for the cyclic temperature experiments. The atmospheric temperature ranged from 10 – 26°C and 16 – 26°C for the unrestrained and restrained energy piles, respectively, during the cyclic heating/cooling experiments. The inlet fluid temperatures were set through the heating/cooling equipment and were generally larger than the atmospheric temperatures; hence the daily natural fluctuations in the atmospheric temperatures did not cause changes in the inlet fluid temperatures. The differences in the fluid types and temperatures were eliminated through numerical modelling by simulating the same type of fluid (water) with the same inlet temperatures, as explained below.

Numerical Modelling

A numerical investigation was conducted to complement the field data and to assess the soil temperature distribution at multiple depths and radial distances from the edge of the two energy piles for the same thermal loads applied to the two energy piles. The numerical investigation was conducted using COMSOL Multiphysics software by modelling the two energy piles under boundary and test conditions representative of the field and validating the numerical model results against the field measurements. Furthermore, parametric investigations on the impact of the same thermal loads and different cyclic temperature variations of the two energy piles on the ground temperature distribution were conducted using the validated model.

A three-dimensional finite element model was developed to analyze the heat transfer between the HDPE pipes, the pile concrete, and the surrounding soil. The heat transfer mechanism between the pile and the ground was assumed to be primarily by conduction due to the absence of groundwater flow. The possible impacts of water phase change and water vapor convection were not included in this analysis, but the thermal properties used in the numerical model are effective values intended to represent those of the unsaturated soils. It was assumed that the soil and concrete pile domains are conductive, isotropic and porous materials filled with air. The governing equations used to solve the present heat transfer problem are commonly used in energy pile analyses (e.g., Batini et al. 2015; Caulk et al. 2016).

The heat conduction equation, assuming no internal heat generation, is written as follows:

$$(\rho C)_{eff} \frac{\partial T}{\partial t} = -\nabla . \lambda_{eff} \nabla T \qquad (1)$$

where $(\rho C)_{eff}$ and λ_{eff} are the effective volumetric heat capacity at constant pressure and effective thermal conductivity, respectively; and T is temperature.

For water circulating in the pipes, the energy conservation equation is written as follows:

$$\rho_f A C_f \frac{\partial T_f}{\partial t} + \rho_f A C_f u_f . \nabla T_f = \nabla . \left(A \lambda_f \nabla T_f \right) + Q_{wall} \qquad (2)$$

where ρ_f, C_f, u_f, λ_f and T_f are density, specific heat, velocity vector, thermal conductivity, and temperature of the circulating fluid, respectively, A is the cross-section of the pipe in which fluid is flowing and Q_{wall} is the heat flux per unit length of pipe, calculated as follows:

$$Q_{wall} = h_{eff}(T_{ext} - T_f) \tag{3}$$

where h_{eff} is the effective pipe heat transfer coefficient considering the wetted perimeter of the pipe cross-section and T_{ext} is the external temperature surrounding the pipe. The effective heat transfer coefficient for circular pipe shapes is calculated as follows:

$$h_{eff} = \frac{2\pi r_{int}}{\frac{1}{h_{int}} + \frac{r_{int}}{\lambda_p}\ln\left(\frac{r_{ext}}{r_{int}}\right)} \tag{4}$$

where r_{int} and r_{ext} are internal and external pipe radius, respectively, λ_p is pipe thermal conductivity, and h_{int} is the convective heat transfer coefficient inside the pipe calculated as follows:

$$h_{int} = \frac{Nu\lambda_f}{d_h} \tag{5}$$

where d_h is the hydraulic diameter ($d_h = \frac{4A}{2\pi r_{int}}$) and $N_u$is the Nusselt number for round pipes, which is defined as a function of the Reynolds, R_e, and Prandtl, P_r, numbers written as follows:

$$Nu = \max\,(3.66; Nu_{turb}) \tag{6.a}$$

$$Nu_{turb} = \frac{\left(\frac{f_D}{8}\right)(R_e - 1000)P_r}{1 + 12.7\sqrt{\frac{f_D}{8}}(P_r^{\frac{2}{3}} - 1)} \tag{6.b}$$

$$f_D = [-1.8\log\left(\frac{6.9}{Re}\right)]^{-1} \tag{6.c}$$

where f_D is friction factor; $Re = \rho VD/\mu$, $Pr = \mu C_f/\lambda_f$, ρ is the fluid density, V is velocity of the fluid, μ is dynamic viscosity of the fluid, D is pipe diameter, C_f is specific heat, and λ_f is the thermal conductivity.

All boundary conditions, pile dimensions, atmospheric temperatures, and inlet fluid temperatures and flow rates were applied to the numerical models using corresponding field data. The 3D simulations for both energy piles were done using a 30 m × 30 m × 40 m (L × W × H) domain shown in Figure 5. The models were characterized by 127365 mesh elements from which 46665 mesh elements described the two energy piles. For the restrained energy pile installed under the building, a slab (with dimensions of 20 m × 20 m × 0.5 m) was assigned at the pile head which increased the number of mesh elements to 128435. A surface to ambient radiation boundary condition was considered at the top surface of the models, and atmospheric temperatures were applied to this surface to account for climatic temperature changes. The surface emissivity coefficients for the unrestrained and restrained energy piles were 0.9 and 0.1, respectively. These values were determined based on the validation of the numerical model with the field data. The effects of other atmospheric processes such as air-soil convective heat transfer, rain, humidity and solar radiation were not considered in this study.

The temperatures at the sides and bottom of the domains were constant and equal to the initial ground temperatures recorded at the beginning of each experiment. Water was used as the heat transfer fluid for all numerical simulations, even though a mixture of antifreeze and water was used in the cyclic experiments of the restrained energy pile. The effect of the antifreeze on the ground temperature responses is assumed to be negligible since a good match between experimental and numerical results was obtained (Figure 6 and Figure 7). Batini et al. (2015) showed that variations in antifreeze compositions have insignificant effects on pile temperature variations. Furthermore, numerical investigations were conducted using the validated models for the same fluid properties (water) and inlet temperatures for the two energy piles

The soil, energy pile, slab and HDPE pipe properties were from Tables 1 and 2 and from previous studies conducted on the two energy piles (Barry-Macaulay et al. 2013; Singh et al. 2015; Yu et al. 2015; Faizal et al. 2018; Faizal et al. 2019a, 2019b). The material properties used in the numerical models are summarized in Tables 4 and 5.

Numerical Validation of Field Results

The transient pile and ground temperatures from the field tests are compared with numerical results between depths of 5 m to 6 m in Figure 6. The in-situ ground temperatures are shown at R = 0.5 m (BH1) and R = 2 m (BH2) for the unrestrained energy pile and at R = 0.63 m (BH1) and R = 1.95 m (BH2) for the restrained energy pile (these locations are shown in Figure 1). Monotonic heating induced higher ground temperatures at BH1 compared to the cyclic temperature changes of the two energy piles. The ground temperature changes are minimal and closer to initial ground temperatures at BH2 for all experiments. It is possible that the ground temperature changes at BH2 could change for long-term operations, particularly for monotonic heating where heat is continuously injected into the ground. But cyclic heating/cooling would still be expected to induce lower ground temperatures compared to monotonic heating for long-term operations. The pile and ground temperature changes for the restrained energy pile, shown in Figure 6d, are lower than that of the unrestrained energy pile shown in Figure 6c due to differences in the fluid temperatures in the cyclic heating/cooling experiments. Due to larger temperature amplitudes of inlet fluid temperatures in the unrestrained pile cyclic experiments, the ground temperature changes at BH1 of the unrestrained energy pile (Figure 6c) were slightly larger than that of BH1 of the restrained energy pile (Figure 6d). The transient numerical results shown in Figure 6 agreed well with the pile and ground temperature measurements for all experiments.

The numerical and experimental pile and ground temperature variations with depth for both energy piles, at Day 15 of operation, are compared in Figure 7. The temperatures are presented at the end of heating and cooling for the cyclic temperature experiments. The ground temperatures remain unchanged below the length of the thermally active loops for all experiments at depth, d =16 m and d = 12 m for the unrestrained and restrained energy piles, respectively. Monotonic heating experiments induced higher ground temperatures at BH1 than almost negligible changes at BH2 at all depths for both energy piles (Figure 7a and Figure 7b). Insignificant ground temperature changes were observed at all depths at both radial locations for the cyclic temperature experiments of the restrained energy pile (Figure 7d). The results from numerical simulations matched well with field results for all depths and radial locations.

Parametric Evaluations

The validated numerical models were used to investigate the radial and vertical ground temperature variations around the two energy piles for the same inlet fluid (water) temperatures, ground and atmospheric temperatures, shown in Figure 8. The inlet fluid temperatures were approximately 35°C for heating simulations and between 10 – 35°C for the cyclic heating/cooling simulations. These temperatures represent the typical range of fluid temperatures encountered in energy piles. The fluid flow rate was 11 LPM. The effects of different frequencies of temperature cycles on the ground temperature variations were also investigated.

Radial and Vertical Ground Temperature Distribution

Time series of the pile and ground temperatures at a depth of 6 m and at different radial distances from the edge of the two energy piles are shown in Figures 9 and 10. This particular depth was selected as it was closer to the middle of both the piles with a similar soil layer consisting of unsaturated dense sand with traces of clay (Tables 1 and 2). Even though the same inlet fluid temperatures were applied to the two energy piles, the pile and ground temperature changes are slightly larger for the restrained energy pile due to the higher number of heat exchanger loops, and thus, higher surface area and higher heat transfer.

A 3D contour plot of ground temperatures at every 0.2 m radial distance from the edge of the energy piles, *R*, is plotted in Figure 9 for qualitative analysis and visualization of radial temperature distribution around the energy piles (pile temperatures are shown at R = 0 m). As expected, the most significant ground temperatures are closer to the energy piles and reduce with increasing radial distance for all simulations. There are noticeable differences in ground temperatures between monotonic and cyclic temperature simulations. The monotonic temperature simulations lead to higher ground temperature changes due to continuous active heat injection in the ground. Therefore, cyclic temperature operation modes of the GSHP will develop lower radial ground temperature changes compared to monotonic temperatures during long-term operations, reducing the possibility of thermal interactions with nearby energy piles.

The time series of pile and ground temperatures are plotted in Figure 10 for quantitative analysis of the radial thermal influence zone. Frequent temperature reversals of the energy piles above and below the initial pile temperatures in the cyclic mode (Figure 10c and 10d) frequently reverse the thermal gradient between the pile and the ground and hence develop much lower changes in ground temperatures than the monotonic heating mode (Figure 10a and 10b). The largest ground temperatures are observed near the energy piles at R = 0.2 m for all simulations, with monotonic heating leading to higher ground temperatures at all radial distances than cyclic heating/cooling. The piles temperature amplitudes at the end of heating and cooling for cyclic simulations get transferred to the soil in the immediate vicinity of the piles but at much lower magnitudes (Figure 10c and Figure 10d). These ground temperature amplitudes are largest near the energy pile at R = 0.2 m and reduce with increasing radial distance and become negligible at R = 2.2 m for both energy piles.

The changes in pile and ground temperatures, ΔT, with respect to initial ground temperatures at Day 15 of operation for all simulations are plotted against radial distance in Figure10e. The radius of the thermal influence zone where the ground temperature changes are greatest is up to 0.4 m for the cyclic temperature experiments for both piles; the ΔT magnitudes after R = 0.4 m remain closer to zero with increasing radial distance. The ΔT magnitudes for monotonic heating also reduce gradually with increasing radial distance but are larger than cyclic heating/cooling for corresponding radial distances. These results indicate that a low volume of soils is thermally affected during cyclic heating/cooling compared to monotonic temperatures. Thus, cyclic temperatures reduce the soil radial thermal influence zone compared to monotonic temperature changes of energy piles under given thermal loads.

Lower radial thermal influence zone during frequent cyclic temperatures in intermittent operations of energy pile systems can be beneficial for designing and applying closely spaced multiple energy piles in real operations. It would cause lower ground temperature changes and reduce or eradicate any thermal interactions between the energy piles via the surrounding soil for long term operations. Previous numerical and field studies (e.g., Di Donna et al. 2016; Mimouni and Laloui 2015) indicated that monotonic heating of a group of closely spaced energy piles develops higher ground temperature changes than heating isolated energy piles. Further, You et al. (2014) reported field studies have also shown that ground temperatures around individual energy piles in closely spaced piles in a group can overlap during monotonic heating. This can cause an overall increase or decrease of ground temperatures and reduce the heat exchange capacity of the energy piles. The results in Figures 9 and 10 show that cyclic temperature operations of the GSHP can help reduce thermal interactions between energy piles in groups since, unlike borehole heat exchangers, the spacing between energy piles cannot be readily increased as it is selected based on structural requirements and not on geothermal energy usage requirements.

The ground temperatures in the two cyclic experiments are presented at the end of heating and cooling (Figures 11c and 11d). The ground temperatures are shown versus depth in Figure 11 at Day 15 of operation to gain more insight on the effects of pile end boundary conditions on the vertical ground temperature distributions. The results confirm that the magnitudes of ground temperature changes reduce with increasing radial distance, and that cyclic heating/cooling develop lower changes compared to monotonic temperatures.

The results in Figure 11 indicate that the boundary conditions at the toe of both piles have a noticeable effect on the ground temperature distribution. The ground temperature changes for all experiments occur up to the depth of installation of the HDPE pipes in the two piles (i.e. along the length of the heat source). As highlighted earlier, minor ground temperature changes are recorded below the length of the thermally active loops at depths of 16 m and 12 m for the unrestrained and restrained energy piles, respectively. Lower ground temperature changes are observed at the end of the loops at 14.2 m and 10 m depths for the unrestrained and restrained energy piles, respectively. The ground temperature changes, and hence the radial thermal influence zone, at the end of the HDPE pipe loops, are lower than those along the thermally active length of the HDPE pipes and become negligible with increasing depths below the HDPE pipes. The heat transfer between the energy piles and the ground and the radial thermal influence zone of the surrounding soil is, therefore, dominant along the active thermal length of the HDPE pipes for both monotonic and cyclic temperature changes of both the piles in the current site soil profile.

The presence of the building cover did not significantly affect the ground temperatures near the pile head, as was observed near the pile toe. This is because the near-surface soil is still in direct contact with the thermally active section of the energy pile. It is possible that internal building activities could have added additional temperature variations to the soil surrounding the restrained energy pile. The effects of the building cover on the vertical ground temperature distribution are slightly evident with monotonic heating of the two energy piles (Figure 11a and Figure 11b); the trends are not so apparent in the cyclic temperature experiments due to the relatively lower magnitudes of ground temperature changes resulting from frequent thermal cycles.

The ground temperatures for the unrestrained energy pile for monotonic heating (Figure 11a) were influenced by the atmosphere up to the depth of 2 m. The near-surface ground temperatures for the restrained energy pile during monotonic heating (Figure 11b) did not appear to have atmospheric effects, indicating that the building cover has some effect in reducing atmospheric effects on the near-surface ground temperatures. Therefore, the effects of the building cover should still be considered when designing real energy pile systems, even though they are not as significant as the effects of the near toe boundary conditions.

The results shown in Figure 11 generally indicate that the vertical ground temperature distribution and the radial thermal influence zone are dominant along the thermally active HDPE pipe length. They depend on the operating modes of the GSHP and magnitudes of pile temperature changes. Also, the pile end boundary conditions do not affect the ground temperature distribution along the thermally active length of the heat exchanger loops (i.e., 14.2 m and 10 m thermally active lengths for the unrestrained and restrained energy piles in this study, respectively). Hence, the atmospheric temperature variations are insignificant and may not have significantly affected the near-surface soil temperatures, as could be the case between different seasons. Further studies are required for long term experiments between different seasons since any given experiment presented in the current study falls within the same season due to the short duration of the tests.

Effect of Varying Frequencies of Daily Cyclic Temperatures

The effects of different cyclic temperatures on the radial ground temperature distribution were investigated by varying the ratio of heating to cooling times. As indicated previously, field and numerical simulations were conducted for 16 hours of cooling followed by 8 hours of heating for both piles (referred to as 16C8H). An additional daily cyclic cooling/heating case was simulated, which cooled the piles for 8 hours, followed by 16 hours of heating (8C16H). The maximum and minimum inlet fluid temperatures at the end of heating and cooling, respectively, were the same as those shown in Figure 8 (i.e., ranging from 10 – 35°C).

The radial ground temperature changes for different temperature cycles of the restrained and unrestrained energy piles at a depth of 6 m are shown in Figure 12. As indicated earlier, the temperature change for the restrained energy pile for a given simulation is higher than the restrained energy pile due to the higher number of heat exchanger loops in the restrained energy pile. The largest effects of different cyclic temperatures on the ground are closest to the pile at R = 0. 2 m and reduce after R = 0.4 m for both energy piles. Negligible ground temperature changes are observed at R = 2.2 m for both piles and cyclic modes.

The 8C16H cyclic mode imposed higher ground temperature changes compared to the 16C8H cyclic mode. This occurred due to the differences in temperatures between the fluid and the ground at the end of cooling and end of heating and differences in the ratio of heating to cooling times. The initial ground temperature at this depth was approximately 17°C for both piles and cyclic modes. Hence, the fluid and ground temperature differences were 18 and 7°C at the end of heating and cooling, respectively, for any given cyclic mode. Therefore, the ground temperature variations were heating dominated in both cyclic simulations. Thus, a larger heating time in the 8C16H mode led to an overall increase in the ground temperatures with operating time. The higher ground temperatures observed in the 8C16H cyclic mode indicate that a larger volume of soil is thermally affected by the operation of the pile compared to the 16C8H mode. Hence, it can be inferred that the radial thermal influence zone is also higher for the 8C16H cyclic mode compared to the 16C8H mode. Therefore, the cooling to heating time ratio per day during cyclic heating/cooling plays a key role in the amount of change of ground temperatures. An implication of this observation is that the ratio of heating to cooling times during cyclic temperature operations of GSHP systems should be selected carefully to avoid unexpected heat gains or losses in the soil.

Conclusions

This paper examined the effects of monotonic and daily cyclic temperature changes and the building cover and near toe boundary conditions on the ground temperature distribution around two separate field-scale energy piles. Conducting an experimental program at a field-scale of the types reported in this paper is challenging since it is difficult to replicate the same boundary conditions such as atmospheric conditions, inlet fluid temperatures and flow rates, operating hours, pile installation technique, pile dimensions and concrete properties, locations of sensors, number of heat exchanger loops, and having same soil properties at corresponding depths. Regardless of the limits in controlling some of the boundary conditions and test variables, the field-scale results were successfully validated with numerical modelling. The combined results provide valuable insight into the effects of temperature cycles and pile end boundary conditions on the soil thermal response.

The soil temperature changes were greatest near the energy piles and reduced with increasing radial distance, with monotonic heating imposing higher ground temperature changes compared to cyclic temperature changes of the energy piles. The radial thermal influence zone of the soil was lower for daily cyclic temperature changes than monotonic heating for given thermal loads. This indicates that cyclic temperature operating modes of the GSHP would affect a lower volume of soils and, hence, reduce thermal interactions with nearby energy piles compared to monotonic temperatures for long term operations. The ground temperature variations were dominant along the length of the thermally active heat exchanger loops. The magnitudes of ground temperature changes were found to be primarily dependent on the operating modes of the energy piles and magnitudes of pile temperature changes. An assessment of the effect of frequencies of daily cyclic temperatures indicates that the heating to cooling ratio can influence the ground radial thermal zone. These frequencies should be selected carefully to avoid unexpected temperature changes of the ground during the cyclic operating modes of the GSHP.

The pile-end boundary conditions affected the ground temperature distributions and should thus be accounted for when designing energy pile systems. The presence of the building cover on the restrained energy pile slightly reduced the atmospheric effects on the vertical soil temperature distribution near the surface compared to the unrestrained energy pile without building cover. The near toe boundary conditions significantly affected the ground temperature distributions since negligible ground temperature changes were observed below the heat exchanger loops. For a given heat input, the ground temperature changes were dominant along the thermally active length of the heat exchanger with lower temperatures near the toe. Therefore, the near toe thermal effects can be neglected when accounting for the effective thermal length of the heat exchanger. Finally, the results presented in this paper are for short-term studies on isolated energy piles. Further long-term studies are required considering seasonal effects on closely spaced energy piles in groups representing real operating systems.

Data Availability Assessment

Some or all data, models, or code that support the findings of this study are available from the corresponding author upon reasonable request.

Acknowledgements

This research project was supported by the Australian Research Council's Linkage Projects funding scheme (project number LP120200613). The unrestrained energy pile installation was funded by the Victorian Government Sustainability Fund (2009–2012), Vibropile Pty. Ltd., Golder Associates Pty. Ltd., and GeoExchange Australia Pty. Ltd. (Project No. 4678). The U.S. National Science Foundation grant CMMI-0928159 supported the fourth author. The support of all the sponsors is gratefully acknowledged.

References

Barry-Macaulay, D., Bouazza, A., Singh, R. M., Wang, B. and Ranjith, P. G. 2013. “Thermal conductivity of soils and rocks from the Melbourne (Australia) region.” *Eng. Geol.* 164 (Sep): 131 – 138. https://doi.org/10.1016/j.enggeo.2013.06.014

Batini, N., Rotta Loria A.F., Conti, P., Testi, D., Grassi, W. and Laloui, L. 2015. “Energy and geotechnical behaviour of energy piles for different design solutions”. *Appl. Therm. Eng.* 86 (Jul): 199 – 213. https://doi.org/10.1016/j.applthermaleng.2015.04.050

Bourne-Webb, P. J., Amatya, B., Soga, K., Amis, T., Davidson, C. and Payne, P. 2009. “Energy pile test at Lambeth College, London: geotechnical and thermodynamic aspects of pile response to heat cycles.” *Géotechnique*, 59 (3): 237 – 248. https://doi.org/10.1680/geot.2009.59.3.237

Brandl, H. 2006. “Energy foundations and other thermo-active ground structures.” *Géotechnique*, 56 (2): 81 – 122. https://doi.org/10.1680/geot.2006.56.2.81

Caulk, R., Ghazanfari, E. and McCartney, J.S. 2016. “Parameterization of a calibrated geothermal energy pile”. *Geomech. Energy Environ.* 5 (Mar): 1 – 15. https://doi.org/10.1016/j.gete.2015.11.001

Chen, Y., Xu, J., Li, H., Chen, L., Ng, CWW. and Liu, H. 2017. “Performance of a prestressed concrete pipe energy pile during heating and cooling”. *J. Perform. Const. Fac.* 31 (3): 06017001. https://doi.org/10.1061/(ASCE)CF.1943-5509.0000982

Dai, L., Li, S., DuanMu, L., Li, X., Shang, Y. and Dong, M. 2015. “Experimental performance analysis of a solar assisted ground source heat pump system under different heating operation modes.” *Appl. Therm. Eng.* 75 (Jan): 325-333. https://doi.org/10.1016/j.applthermaleng.2014.09.061

De Moel, M., Bach, P.M., Bouazza, A., Singh, R.M. and Sun, J.O. 2010. “Technological advances and applications of geothermal energy pile foundations and their feasibility in Australia”. *Renewable and Sustainable Energy Reviews* 14(9):2683-2696. https://doi.org/10.1016/j.rser.2010.07.027

Di Donna, A., Ferrari, A. and Laloui, L. 2016. “Numerical study of the response of a group of energy piles under different combinations of thermo-mechanical loads”. *Comput. Geotech.* 72: 126 – 142. https://doi.org/10.1016/j.compgeo.2015.11.010

Faizal, M., Bouazza, A. and Singh, R. M. 2016. “An experimental investigation of the influence of intermittent and continuous operating modes on the thermal behaviour of a full scale geothermal energy pile.” *Geomech. Energy Environ.* 8: 8 – 29. https://doi.org/10.1016/j.gete.2016.08.001

Faizal, M., Bouazza, A., Haberfield, C. and McCartney, J.S. 2018. “Axial and radial thermal responses of a field scale energy pile under monotonic and cyclic temperature changes”. *J. Geotech. Geoenviron. Eng.* 144 (10): 04018072. https://doi.org/10.1061/(ASCE)GT.1943-5606.0001952

Faizal, M., Bouazza, A., McCartney, J.S. and Haberfield, C. 2019a. “Effects of cyclic temperature variations on the thermal response of an energy pile under a residential building”. *J. Geotech. Geoenviron. Eng.* 145 (10): 04019066. https://doi.org/10.1061/(ASCE)GT.1943-5606.0002147

Faizal, M., Bouazza, A., McCartney, J.S. and Haberfield, C. 2019b. “Axial and radial thermal responses of an energy pile under a 6-storey residential building”. *Can. Geotech. J.* 56 (7): 1019 – 1033. https://doi.org/10.1139/cgj-2018-0246

Faizal, M. and Bouazza, A. 2018. “Energy utilization and ground temperature distribution of a field scale energy pile under monotonic and cyclic temperature changes”. In: *Proceedings of China-Europe Conference on Geotechnical Engineering*, Vienna, Austria. Edited by W. Wu and H.-S. Yu . Springer Nature, Switzerland, pp. 1591–1594, 2018. https://doi.org/10.1007/978-3-319-97115-5_151

Ghasemi-Fare, O. and Basu, P. 2018. “Influences of ground saturation and thermal boundary condition on energy harvesting using geothermal energy piles”. *Energy Build.* 165 (Apr): 340 – 351. https://doi.org/10.1016/j.enbuild.2018.01.030

Guo, Y., Zhang, G. and Liu, S. 2018. “Investigation on the thermal response of full-scale PHC energy pile and ground temperature distribution in multi-layer strata”. *Appl. Therm. Eng.* 143 (Oct): 836 – 848. https://doi.org/10.1016/j.applthermaleng.2018.08.005

Jalaluddin, Miyara, A., Tsubaki, K., Inoue, S. and Yoshida, K. 2011. “Experimental study of several types of ground heat exchanger using a steel pile foundation”. *Ren. Energy* 36 (2): 764 – 771. https://doi.org/10.1016/j.renene.2010.08.011

Kaltreider, C., Krarti, M. and McCartney, J.S. (2015). “Heat transfer analysis of thermo-active foundations.” *Energy and Buildings*. 86, 492-501.

Li, X., Chen, Y., Chen Z. and Zhao, J. 2006. “Thermal performances of different types of underground heat exchangers”. *Energy Build.* 38 (5): 543 – 547. https://doi.org/10.1016/j.enbuild.2005.09.002

Mimouni, T. and Laloui, L. (2015). “Behaviour of a group of energy piles.” *Can. Geotech. J.* 52 (12): 1913 – 1929. https://doi.org/10.1139/cgj-2014-0403

Murphy, K. D., McCartney, J. S. and Henry, K. S. 2015. “Evaluation of thermo-mechanical and thermal behavior of full-scale energy foundations.” *Acta Geotech.* 10 (2): 179 – 195. https://doi.org/10.1007/s11440-013-0298-4

Murphy, K. D., and J. S. McCartney. 2015. “Seasonal response of energy foundations during building operation.” *Geotech. Geol. Eng.* 33 (2): 343–356. https://doi.org/10.1007/s10706-014-9802-3

McCartney, J.S. and Murphy, K.D. 2017. “Investigation of potential dragdown/uplift effects on energy piles.” *Geomech. Energy Environ.* 10 (Jun): 21 – 28. https://doi.org/10.1016/j.gete.2017.03.001

Singh, R.M., Bouazza, A. and Wang, B. 2015. “Near-field ground thermal response to heating of a geothermal energy pile: observations from a field test.” *Soils Found.* 55 (6): 1412 – 1426. https://doi.org/10.1016/j.sandf.2015.10.007

Wang, B. 2017. “Behaviour of pile foundations subjected to thermal loading.” Master of Engineering Thesis, Monash University, Melbourne, Australia.

Wang, B., Bouazza, A., Singh, R., Haberfield, C., Barry-Macaulay, D. and Baycan, S. 2015. “Posttemperature effects on shaft capacity of a full-scale geothermal energy pile.” *J. Geotech. Geoenviron. Eng.* 141 (4): 04014125. https://doi.org/10.1061/(ASCE)GT.1943-5606.0001266

Wood, C.J., Liu, H. and Riffat S.B. 2010. “Comparison of a modelled and field tested piled ground heat exchanger system for a residential building and the simulated effect of assisted ground heat recharge”. *Int. J. Low-Carbon Technol.* 5 (3): 137 – 143. https://doi.org/10.1093/ijlct/ctq015

Yi, M., Hongxing, Y. and Zhaohong, F. 2008. “Study on hybrid ground-coupled heat pump systems.” *Energy Build.* 40 (11): 2028–2036. https://doi.org/10.1016/j.enbuild.2008.05.010

You, S., Cheng, X., Guo, H. and Yao, Z. 2014. “In-situ experimental study of heat exchange capacity of CFG pile geothermal exchangers.” *Energy Build.* 79 (Aug): 23 – 31. https://doi.org/10.1016/j.enbuild.2014.04.021

Yu, K. L., Singh, R. M., Bouazza, A. and Bui, H. H. 2015. “Determining soil thermal conductivity through numerical simulation of a heating test on a heat exchanger pile.” *Geotech. Geol. Eng.* 33 (2): 239 – 252. https://doi.org/10.1007/s10706-015-9870-z

Table 1. Summary of ground conditions at the test site of the unrestrained energy pile (Barry-Macaulay et al. 2013; Singh et al. 2015; Wang et al. 2015; Yu et al. 2015; Faizal et al. 2018).

Depth [m]	Soil type	Soil description	In situ test values	Gravimetric water content (%)
0 – 1.5	Fill Material	Silty clay with traces of fine gravel and medium-coarse grained sand.	-	20 – 30
1.5 – 2.5	Sandy clay	Clay containing fine-medium grained sand with cemented layers.	c_u = 400 kPa (pocket penetrometer)	12 – 19
2.5 – 10	Sand (with traces of clay)	Fine to coarse-grained sand. Dense from 2.5 m to 4 m and very dense from 4 m to 10 m. Quartz content ≤ 65%.	N = 26 @ 3 m depth N = HB > 3 m depth[a]	5 – 8
10 – 16.1	Sand	Fine to coarse-grained sand. Very dense. Quartz content = 93%.	N = HB[a]	2 – 5

[a] HB (hammer bounce) encountered during SPT tests conducted i.e. N > 50.

Table 2. Summary of ground conditions at the test site of the restrained energy pile (Faizal et al. 2019a, 2019b).

Depth [m]	Soil type	Soil description	In-situ test values	Gravimetric water content (%)
0 – 0.4	Fill material	Crushed rock silt, sand, moist, medium dense	–	–
0.4 – 3.5	Sandy clay	Silt, sand (sand lenses) moist, stiff - very stiff	c_u = 90 – 140 kPa (shear vane test) SPT N = 12 - 27	13 – 24
3.5 – 12.5	Sand	Sand, clay lenses, silt, cemented lenses, moist, dense	SPT N = 25 – 30	5 – 13

SPT N: Standard penetration test blow count.

Table 3. Summary of experiments.

Operating mode	Description	Inlet fluid temperatures [°C]	Inlet fluid flowrates [LPM]	Experiment duration [days]
Unrestrained energy pile heating	24 hours heating, daily	45	10	52
Unrestrained energy pile cyclic	16 hours cooling and 8 hours heating, daily	7 – 16 (cooling cycle) 30 - 55 (heating cycle)	15 (cooling cycle) 13.5 (heating cycle)	24
Restrained energy pile heating	24 hours heating, daily	48	11	18
Restrained energy pile cyclic	16 hours cooling and 8 hours heating, daily	8 (cooling cycle) 30 (heating cycle)	16 (cooling cycle) 16 (heating cycle)	17

Table 4. Material properties used in the numerical simulation of the unrestrained energy pile.

Material	Depth [m]	Porosity n [—]	Total density ρ [kg/m^3]	Specific heat capacity C_p [J/kg.K]	Thermal conductivity λ [W/m.K]
Fill: silty clay	0 - 1.5	0.35	1800	790	1.49
Sandy clay	1.5 - 4	0.35	1750	810	1.5
Sand with clay traces	4 - 8	0.35	1800	800	1.9
Very dense sand	8 - 40	0.3	2100	850	2.4
Pile	—	—	2550	810	1.5
HDPE pipes	—	—	—	—	0.4

Table 5. Material properties used in the numerical simulation of the restrained energy pile.

Material	Depth [m]	Porosity n [—]	Total density ρ [kg/m^3]	Specific heat capacity C_p [J/kg.K]	Thermal conductivity λ [W/m.K]
Fill	0 - 0.5	0.35	1800	800	1.1
Dense sand	0.5 - 3.5	0.33	1950	840	1.7
Dense sandy clay	3.5 - 6	0.33	2050	810	2.2
Very dense sand	6 - 40	0.3	2100	850	2.6
Pile	—	—	2550	810	1.7
Slab	—	—	2600	850	1.7
HDPE pipes	—	—	—	—	0.4

Table 6. Summary of domain sizes and mesh elements used for the cyclic heating/cooling parametric study.

	Restrained energy pile		Unrestrained energy pile	
Pile length [m]	Soil height [m]	Mesh elements	Soil height [m]	Mesh elements
16	40	128435 (46665)	40	127365(46665)
20	50	163952 (54092)	50	162138 (54092)
24	60	200341 (61862)	60	192929 (61862)

Note: Values in parentheses indicate number of mesh elements of the pile domain.

List of Figures

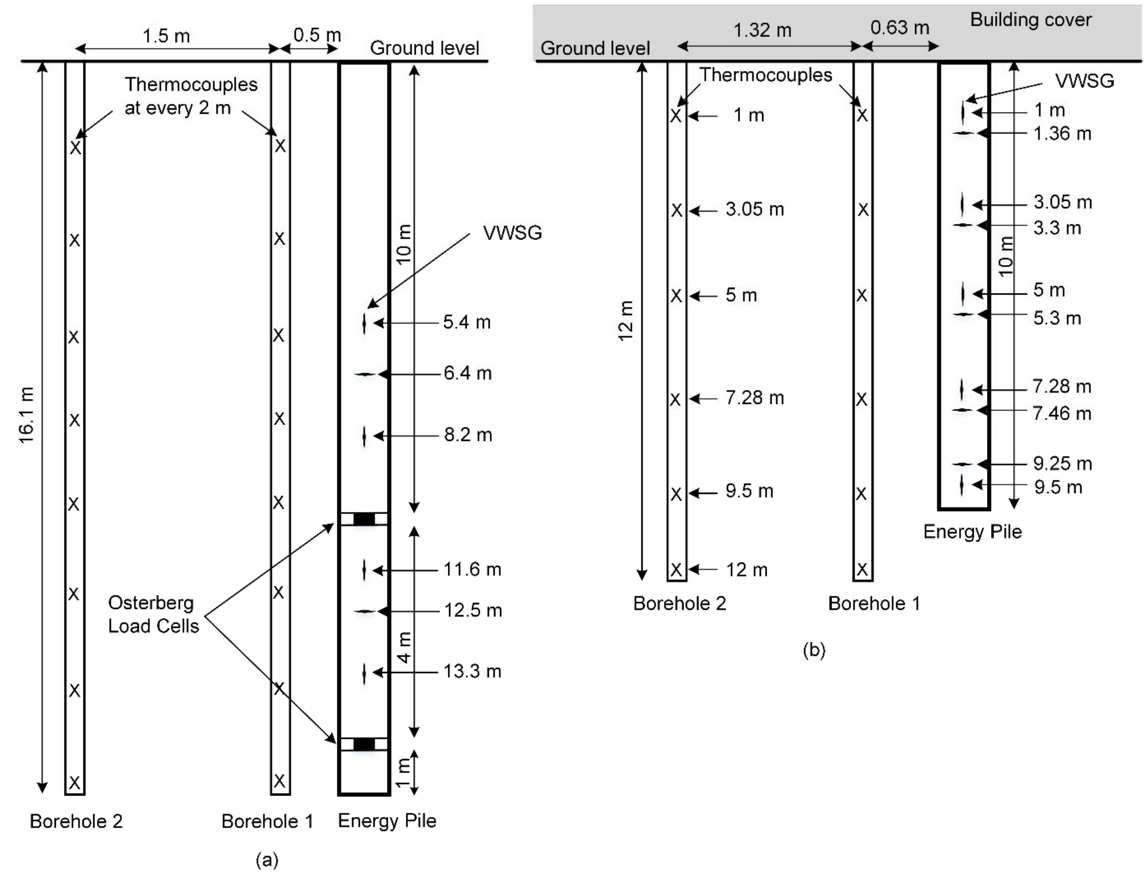

Figure 1. Schematic diagrams of the energy piles: a) energy pile without building cover (unrestrained energy pile), and b) energy pile under the 6-story residential building (restrained energy pile). (VWSG = vibrating wire strain gauge).

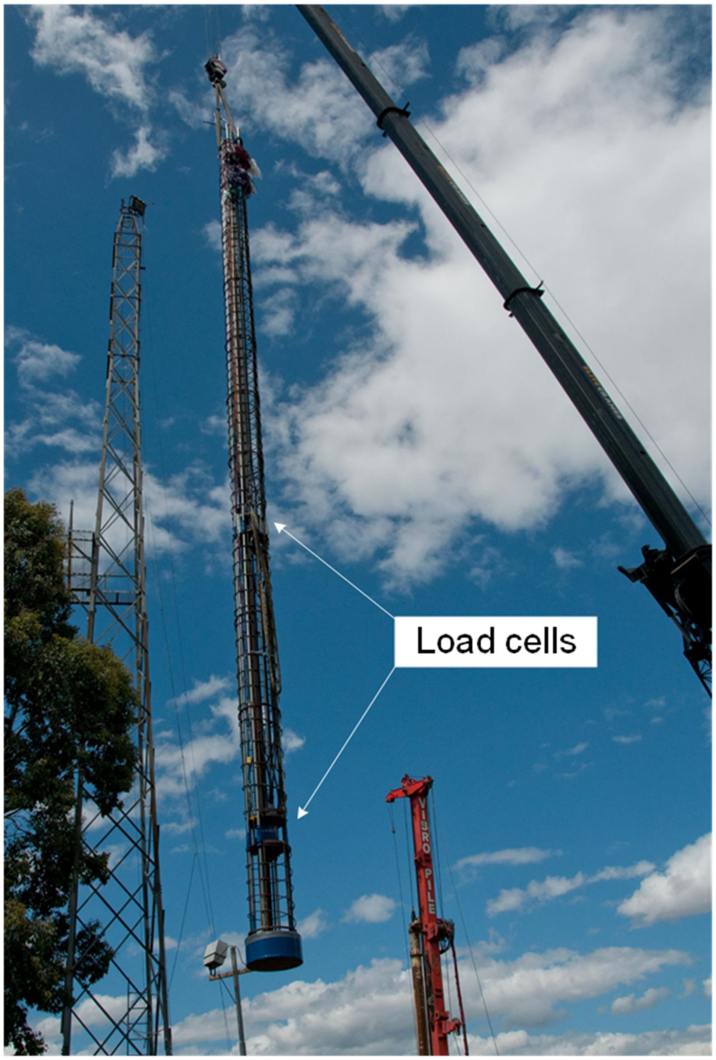

Figure 2. Installation pictures of the energy pile without the building cover (referred to as the unrestrained energy pile): a) Need more installation pics.

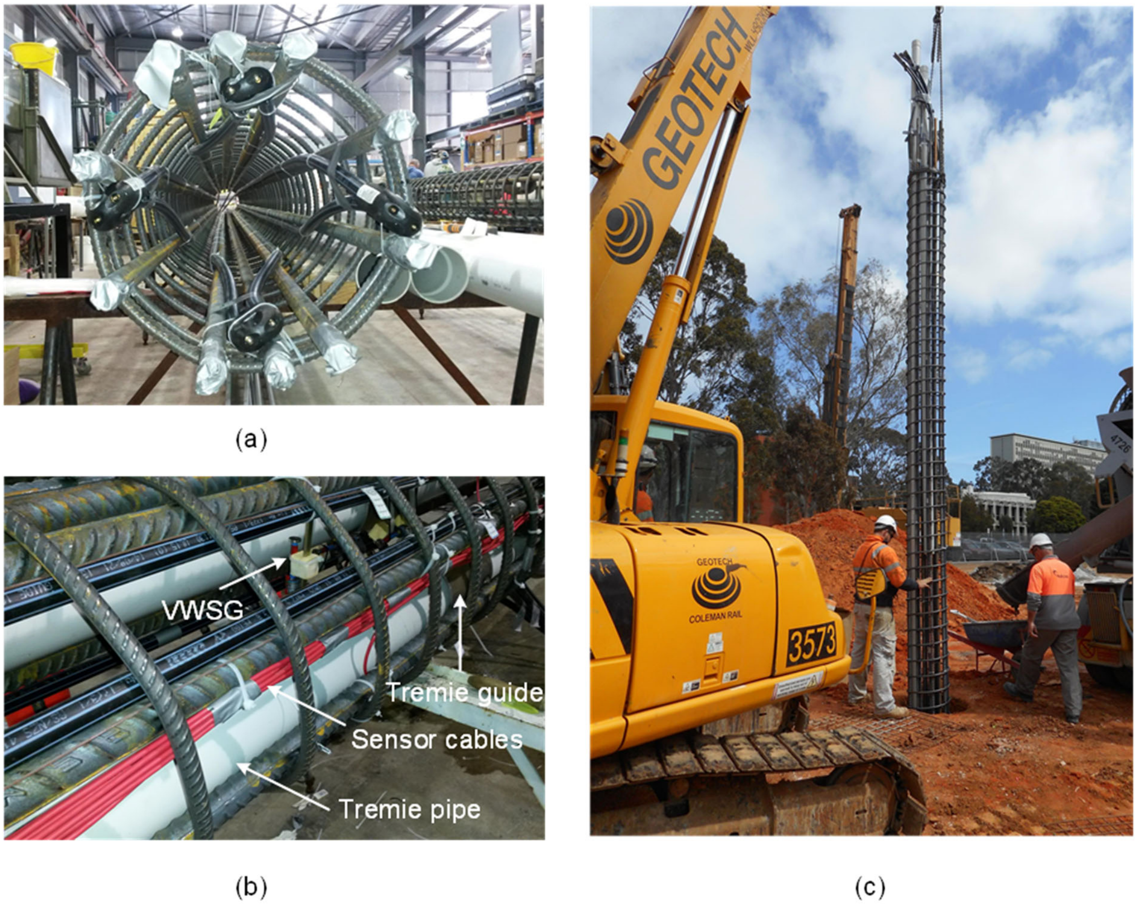

Figure 3. Installation pictures of the energy pile under the building (referred to as the restrained energy pile): a) U-loops in the pile cage, b) pipes, sensors cables, and removable tremies along the pile length, and c) inserting pile-cage in the ground.

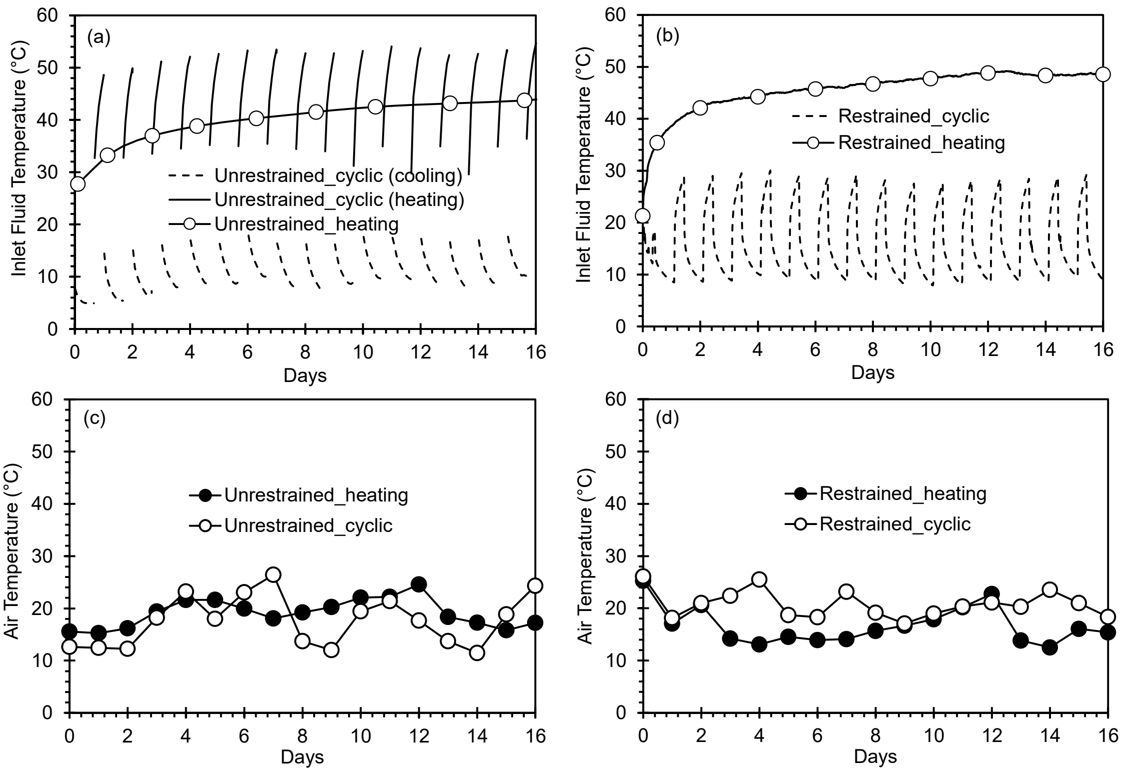

Figure 4. Inlet fluid and daily atmospheric temperatures during experiments: a) inlet fluid temperatures for the unrestrained energy pile, b) inlet fluid temperatures for the restrained energy pile, c) atmospheric temperatures for the unrestrained energy pile, and d) atmospheric temperatures for the restrained energy pile.

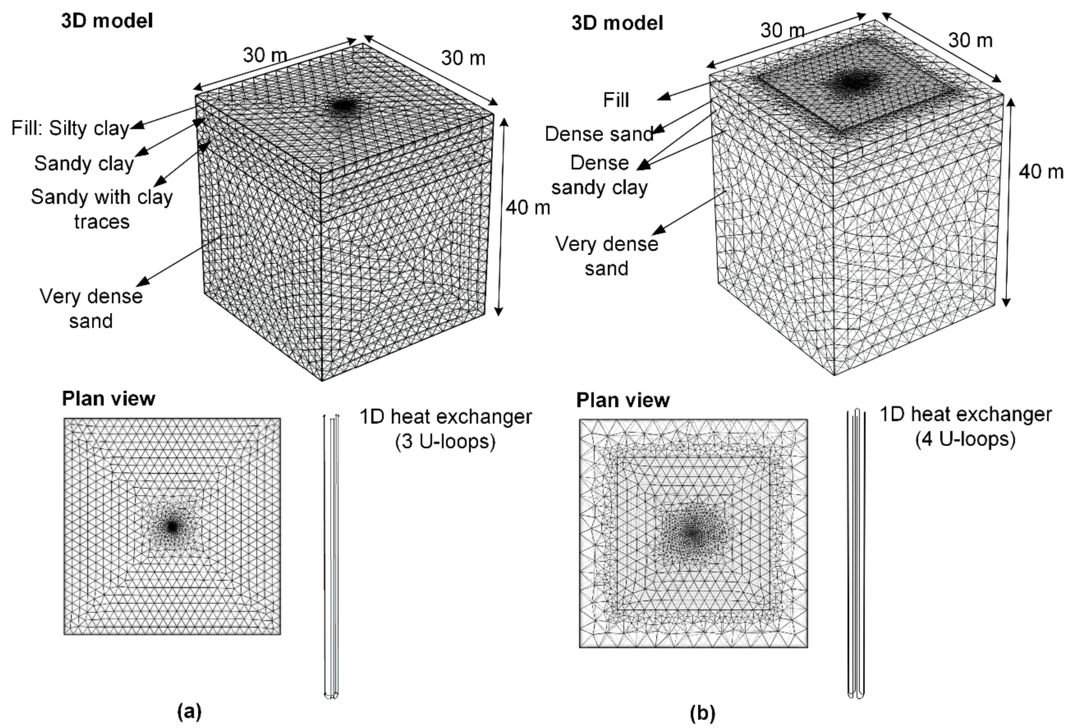

Figure 5. Finite element meshes for the two energy piles: a) unrestrained energy pile, and b) restrained energy pile.

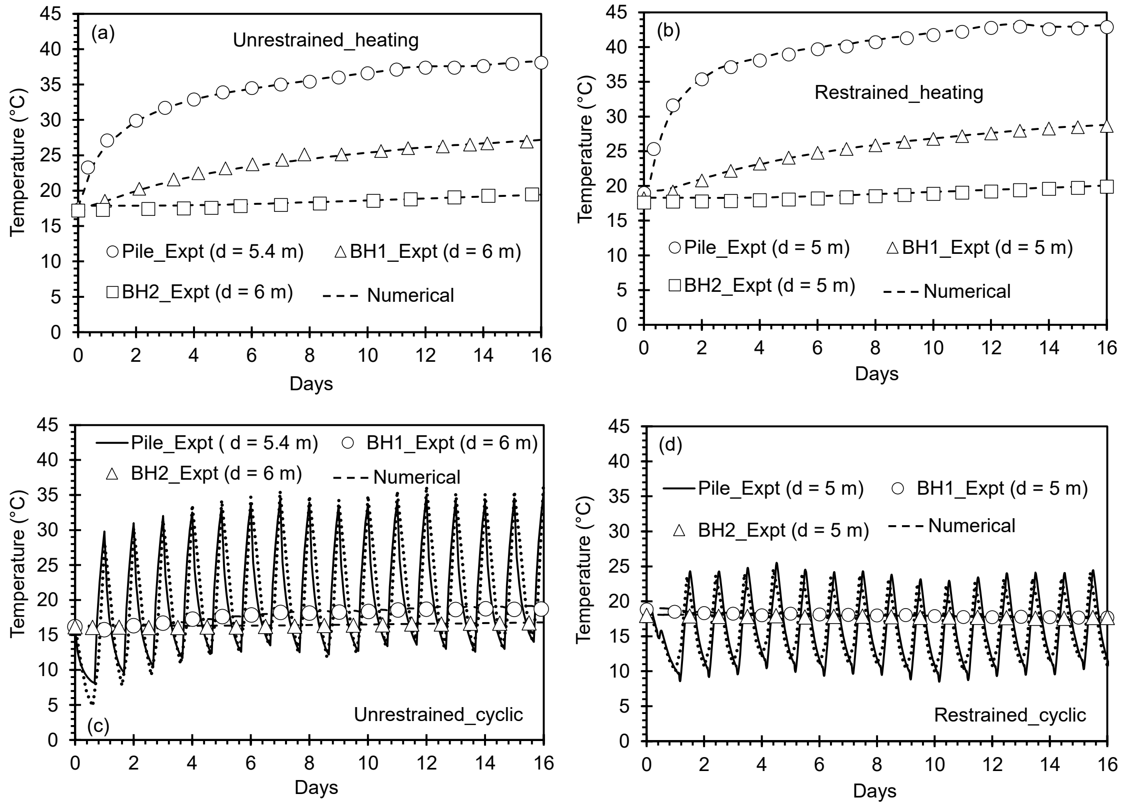

Figure 6. Comparison of numerical and field temperature results as a function of time at depths of 5 m to 6 m: a) monotonic heating of unrestrained energy pile, b) monotonic heating of restrained energy pile, c) cyclic heating/cooling of unrestrained energy pile, and d) cyclic heating/cooling of restrained energy pile.

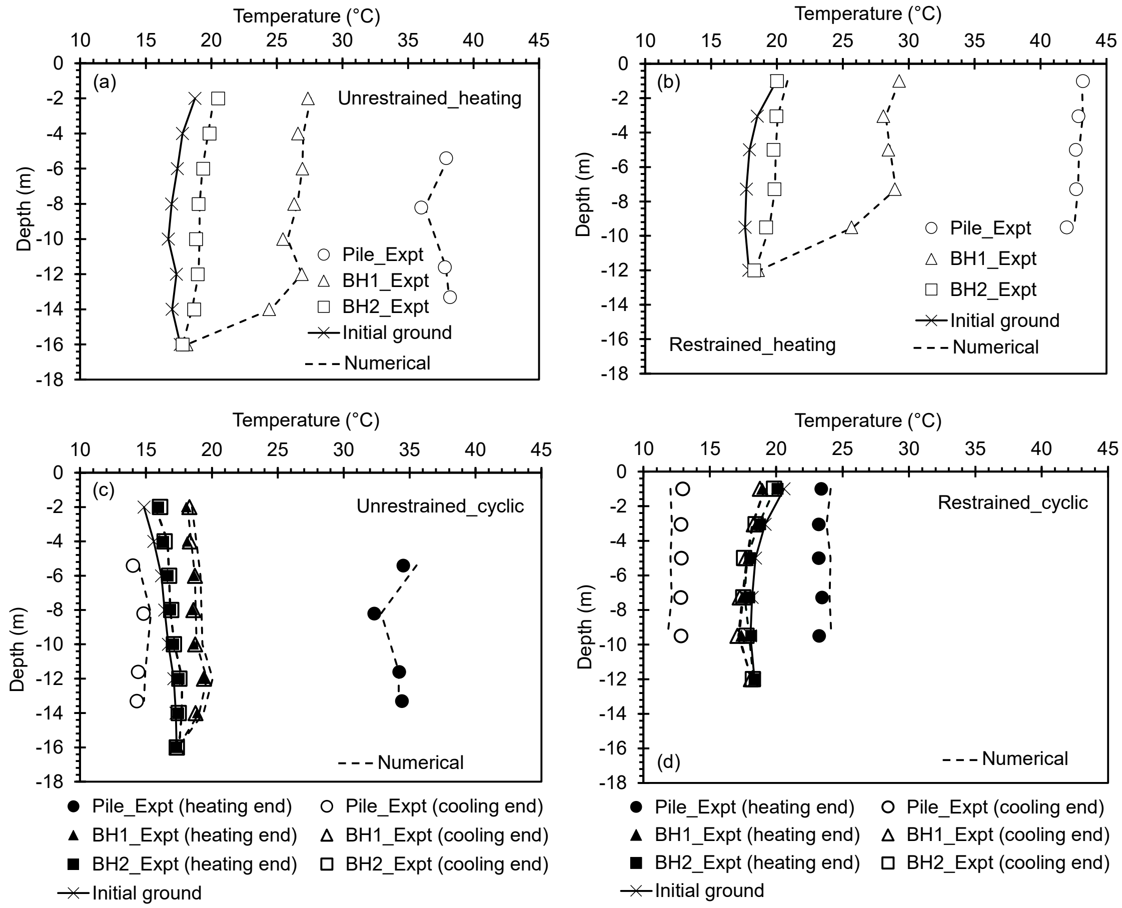

Figure 7. Comparison of numerical and field temperature results as a function of depth: a) monotonic heating of unrestrained energy pile, b) monotonic heating of restrained energy pile, c) cyclic heating/cooling of unrestrained energy pile, and d) cyclic heating/cooling of restrained energy pile.

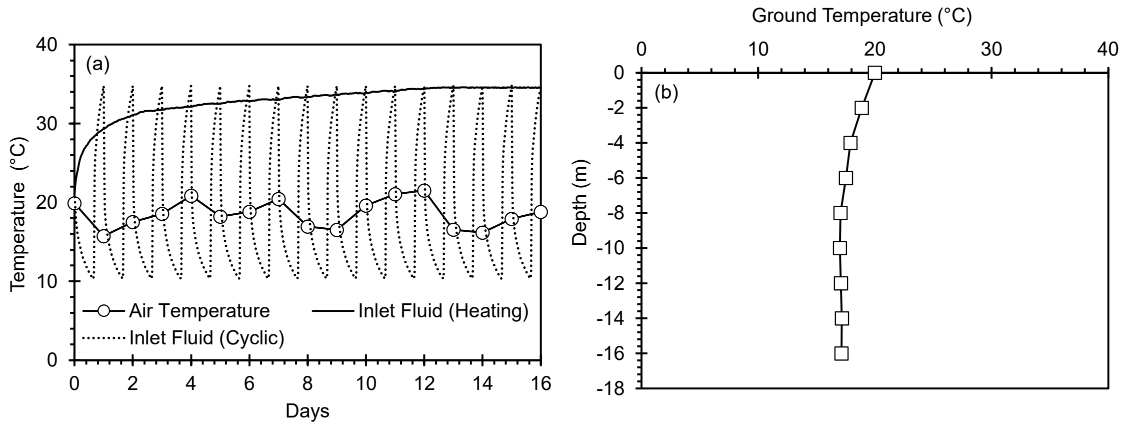

Figure 8. Inlet fluid, air and ground temperatures for parametric evaluations of both energy piles: a) inlet fluid and air temperatures, and b) initial ground temperatures.

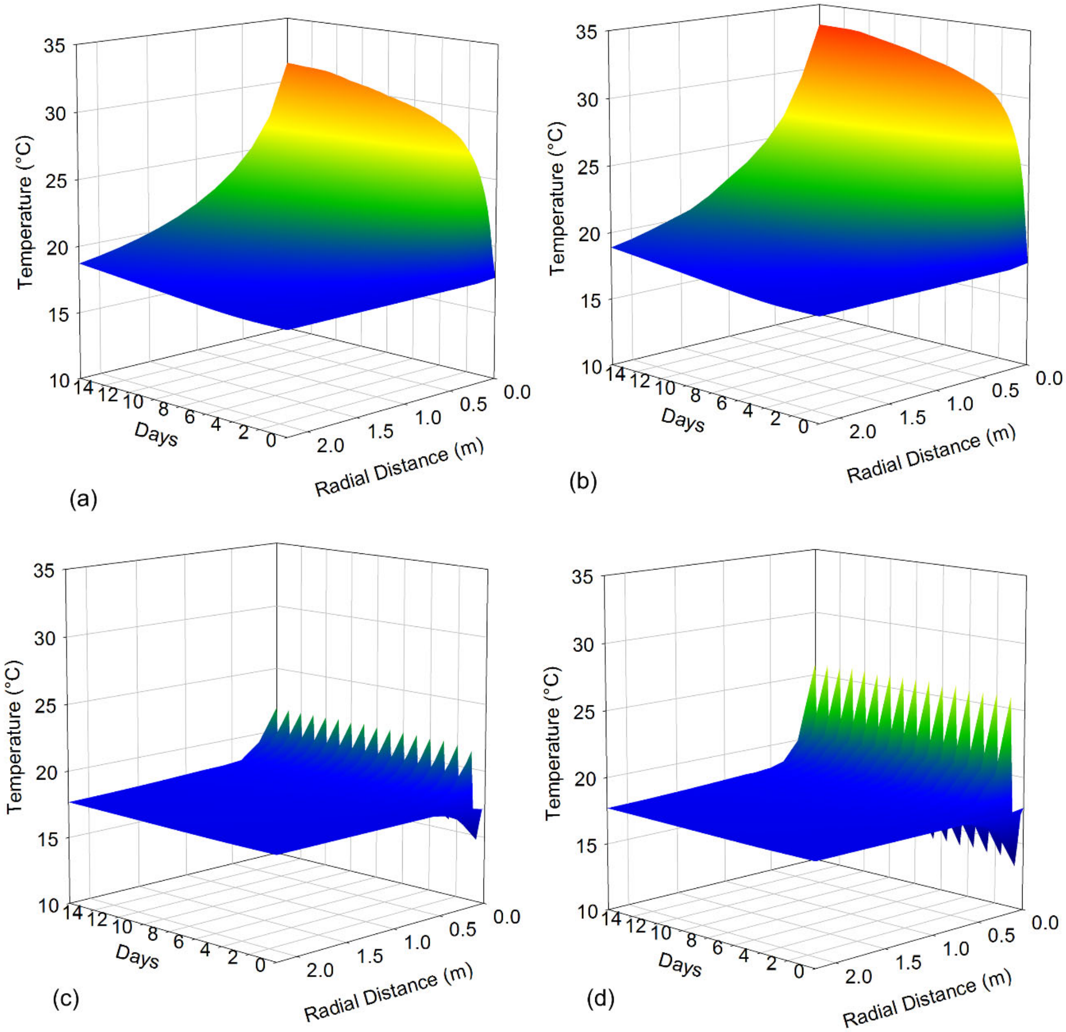

Figure 9. Contours of ground temperatures around the energy piles at a depth of 6 m: a) monotonic heating of unrestrained energy pile, b) monotonic heating of restrained energy pile, c) cyclic heating/cooling of unrestrained energy pile, and d) cyclic heating/cooling of restrained energy pile.

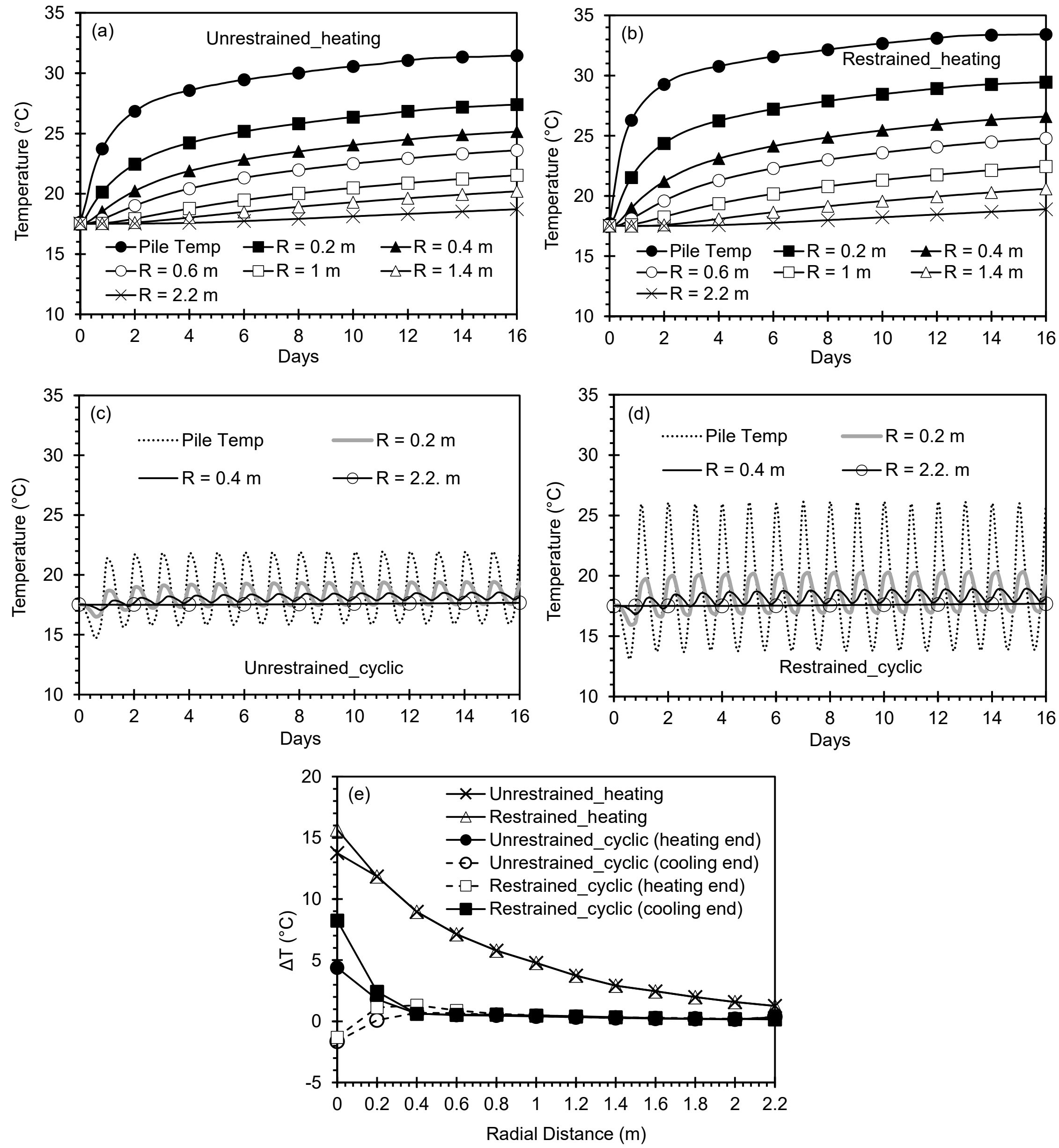

Figure 10. Ground temperatures at different distances, *R*, from the edge of the piles at a depth of 6 m: a) monotonic heating of unrestrained energy pile, b) monotonic heating of restrained energy pile, c) cyclic heating/cooling of unrestrained energy pile, d) cyclic heating/cooling of restrained energy pile, and e) change in pile and ground temperatures with respect to initial conditions at Day 15.

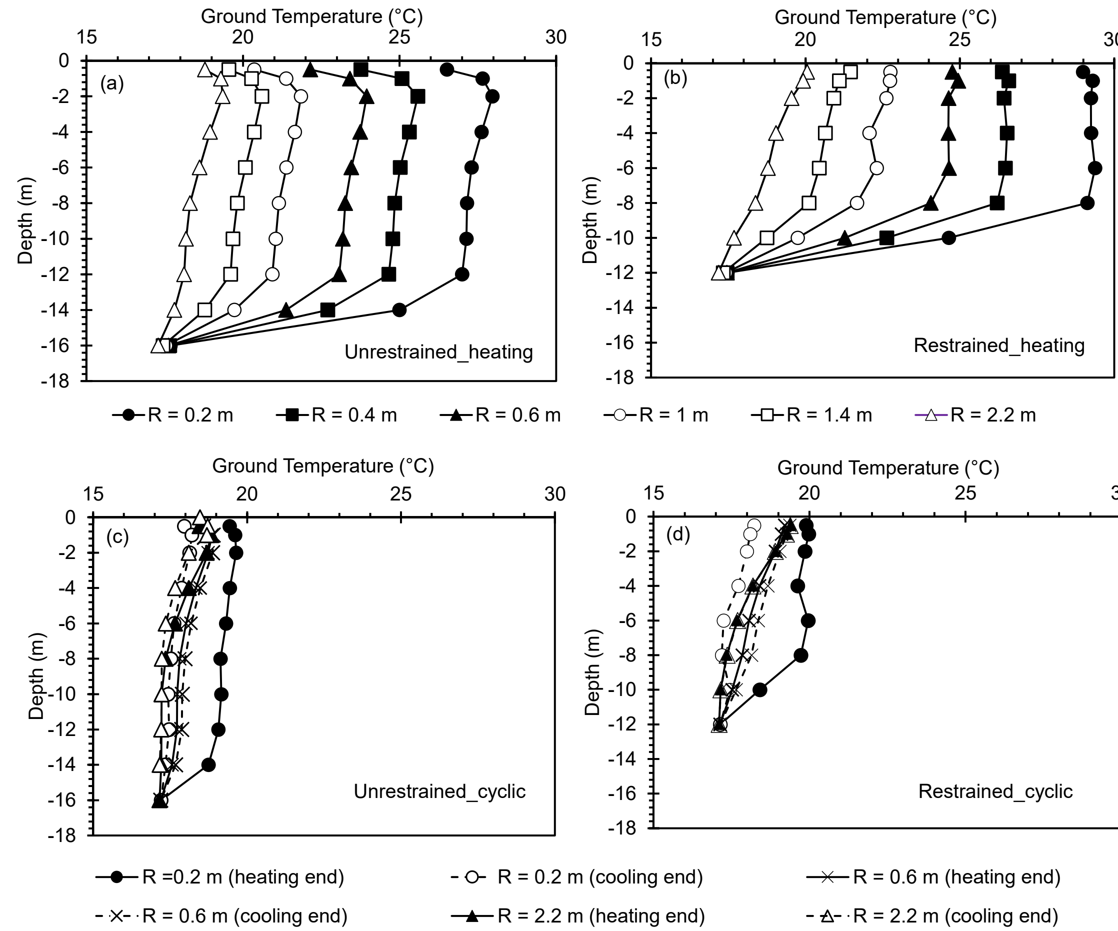

Figure 11. Ground temperatures plotted against depth at different radial distances, *R*: a) monotonic heating of unrestrained energy pile, b) monotonic heating of restrained energy pile, c) cyclic heating/cooling of unrestrained energy pile, and d) cyclic heating/cooling of restrained energy pile.

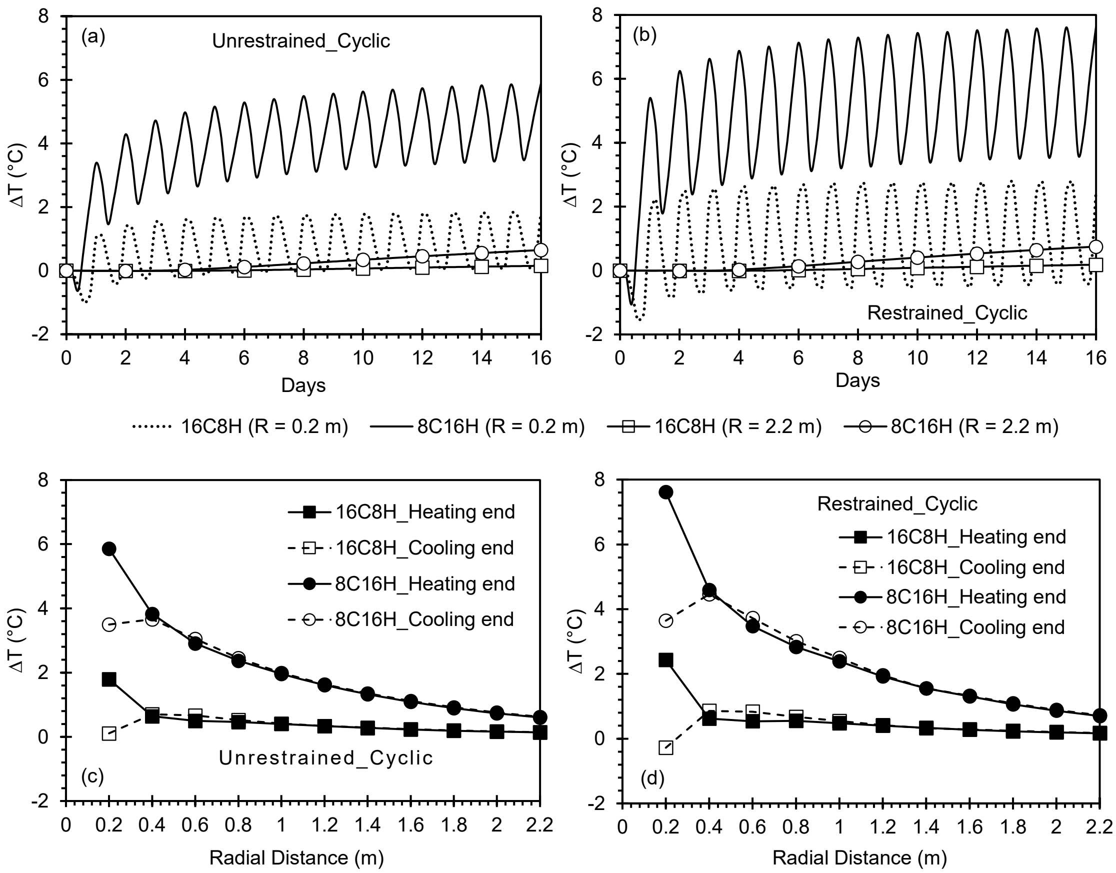

Figure 12. Changes in ground temperatures, ΔT, at different distances, R, from the edge of the energy piles at d = 6 m under different temperature cycles: a) unrestrained energy pile, b) restrained energy pile, c) ΔT of unrestrained energy pile against R, and d) ΔT of restrained energy pile against R.